steel research international
www.steel-research.de

Vacuum Brazing of 18MAR300 Nickel Maraging Steel Joints Based on Additively Manufactured and Conventional Material Grades

Wolfgang Tillmann, Tim Henning, Lukas Wojarski, and Julia Bültena*

Laser powder bed fusion (LPBF) processes offer the best possible design options for the production of highly complex components with unique functionalities. Although the development of additive manufacturing processes is progressing impressively and build rates have already been significantly increased, the economic production of high-volume components is still particularly truncated. Comparatively expensive powders, machine-hour rates, and a limited construction space demonstrate a high demand for joining LPBF components to conventionally manufactured parts. Vacuum brazing is an excellent technology for manufacturing and simultaneous heat treatment of such hybrid components. The aim of this study is to investigate the brazeability and the joint properties of ultrahigh-strength nickel maraging steel 18MAR300 (1.2709, X3NiCoMoTi18-9-5) using BVAg-30 (Ag68Cu27Pd5) as brazing filler metal. For this purpose, the effect of nickel-plated surfaces on the wettability and the microstructure of the joint is studied for conv./conv.-, LPBF/conv.-, and LPBF/LPBF joints. Furthermore, the quasi-static and quasi-dynamic joint strength is evaluated. The results prove that nickel-plated surfaces are vital to achieve a sufficient process control. The coating assures a deoxidized and sealed surface which favors the formation of NiCu(Fe, Pd,Ag) phases within the braze metal thus enhancing the joint strength. In addition, LPBF/LPBF joint features have significantly higher tensile strength than conv./conv. joints (825–627 MPa).

1. Introduction

Vacuum brazing of nickel maraging steels is a great challenge since the materials surface is characterized by a complex oxide layer (Fe_3O_4, TiO_2, MoO_3, and $MoO_3 \cdot xH_2O$), which is, in contrast to stainless steels, even at high vacuum not sufficiently reducible at suitable brazing process temperatures (except of Fe_3O_4).[1–3] The process temperature is limited to 980 °C maximum since a higher temperature leads to significant grain growth, which highly reduces the toughness of the steel.[4–7] Beyond the usually outstanding low-temperature toughness, nickel maraging steels offer more unique material properties such as a ultrahigh tensile strength (up to 2400 MPa) and a particularly homogeneous hardness distribution.[8] Therefore, these steels are primarily used for highly stressed components (e.g., hydraulic chucks, wind tunnel models, and injection molds).[9–11] Most of the common martensitic hardenable steels (e.g., AISI H11, AISI H13) are highly limited to the through hardenability for large components in vacuum furnaces since the cooling rates that can be achieved inside the material are too low to avoid the diffusion of carbon. As a result of the locally different microstructure (martensite and bainaite), the hardness decreases with the distance to the surface. In contrast, nickel maraging steels are precipitation hardenable steels, and thus, the hardness is homogeneous and independent from the component dimension. Nickel maraging steels contain mainly 18% nickel and high concentrations of cobalt and molybdenum as well as one percentage of titanium. In detail, these elements are responsible for the hardness increase during annealing by the formation of Ni_3Mo and Ni_3Ti precipitates, with cobalt significantly reducing the solubility of molybdenum which enhances the total amount of precipitations.[12,13]

Additive manufacturing processes have developed enormously in recent decades. Compared to other methods like direct energy deposition (DED) or binder jetting laser powder bed fusion (LPBF) is much better researched. The processing of nickel maraging steels by LPBF offers an almost free design of the component, which enables unique functions like conformal cooling for injection molds.[13–16] However, the costs of the powder as well as the slow layer by layer process limit an economic production of high-volume components, even with respect to the using of hull-and-core strategy.[17–19] Since the required component functionality is often only required locally, it is obvious to join an LPBF part with high functionality to conventionally produced material (e.g., for clamping of the component).[20–23] As mentioned earlier, the complex oxide layer of maraging steels is difficult to wet by brazing alloys due to the

W. Tillmann, T. Henning, L. Wojarski, J. Bültena
Institute of Materials Engineering
TU Dortmund University
Leonhard-Euler Str. 2, 44227 Dortmund, Germany
E-mail: tim.henning@tu-dortmund.de

The ORCID identification number(s) for the author(s) of this article can be found under https://doi.org/10.1002/srin.202300108.

DOI: 10.1002/srin.202300108

incompatibility of the atomic bonding types (ionic covalent and metallic). Our previous investigations revealed that argon ion etching followed by arc deposition of nickel in vacuum is vital to assure a sufficient wetting and joint quality for conventional AISI 18MAR300 material grades.[24,25] The high kinetic energy of the argon ions removed the oxide layer sufficiently, while the subsequntly applied coating of nickel in the vacuum atmosphere prevented the surface from reoxidation. With respect to the brazing alloy, it was found that palladium acts as a key element for wetting and enhances the tensile strength of the joint by solid solution strengthening of the Ag(Cu,Pd) phase. In this regard, it must be taken into account that the silver-rich matrix of the braze metal is the weak point of the joint. A tensile strength of 659 MPa (SD: 59) was obtained with BVAg-30 (Ag68Cu27Pd5) brazing filler metal using nickel-plated surfaces. In another study, we were able to prove that LPBF/LPBF joints and hybrid joints of LPBF and conventional material grades for AISI 18MAR300 provide a significantly higher tensile strength of 972 MPa (SD: 20) or respectively 904 MPa (SD: 38) when using AuNi18 brazing filler metal which does not require a nickel-plated surface.[17] Furthermore, it was shown that if the LPBF part is directly build-up onto a conventional material grade and then solution annealed and precipitation hardened without brazing, the tensile strength was 1998 MPa (SD: 62). However, it could also be shown that the imperfections within the LPBF microstructure (interlayer defects, unmolten particles, keyhole voids, and oxide inclusions) affect the tensile strength and the increased load fatigue strength as well for the solid material which is also reported by other researchers.[26–29] In this regard, the formation of interlayer defects is well researched, whereas actual findings prove for example the formation of voids by the keyhole effect of the laser which indicates that further research is necessary to understand the effect of such imperfections on further processing technologies like brazing.[30] A study on brazing hybrid LPBF/conv. joints of AISI 316L stainless steel using the nickel-based brazing filler metal AMS 4777 showed that a single-sided pore space was present in the vicinity of the diffusion area for the additively produced part which signficicantly reduced the joint strength.[31] In this regard, the microstructure of the diffusion area differed clearly from the opposite side of the conventional material. As a consequence of all these differences, the corrosion behavior of the joint can be different depending on the material grade used for brazing.[32]

A main point of the present investigations is characterized by the extent to which the microstructure and the strength of the brazed joint are affected by an LPBF or a conventional material grade of AISI 18MAR300. Furthermore, the effect of the imperfections within the LPBF material on the joint quality is of particular interest. Manufacturing processes for the industrial mass production of such components by brazing require comprehensive knowledge of these relationships when different material grades were used.

2. Experimental Section

A conventionally casted rod (ø 20.5 mm) of AISI 18MAR300 was processed to cylindrical samples of diameter 18 mm and height of 50 mm for the brazing samples and height of 100 mm for the solid samples. For the samples with an increasing gap size, a rectangular geometry of 25 mm × 20 mm × 5 mm was used. A gas atomized powder of AISI 18MAR300 with a particle size of +45–15 µm provided by Carpenter Additive was utilized to produce cylindrical and rectangular LPBF samples (ø 22 mm with height 110 mm, 30 mm × 25 mm × 5 mm). These samples were machined to the same dimensions of the conventional ones to remove the surface layer containing high residual stresses and defects with certainty. **Table 1** compares the chemical composition of the different material grades specified by the material quality certificates.

Table 1. Chemical composition of AISI 18MAR300 rod material and LPBF powder.

[wt%]	C	O	Al	Ti	Cr	Mn	Fe	Co	Ni	Mo
Conventional rod	0.002	–	0.04	1.02	0.06	0.02	Bal.	8.79	17.19	4.73
LPBF powder	0.030	0.02	0.10	1.00	0.01	0.02	Bal.	9.80	18.90	5.20

It is noticeable, that the powder used for the manufacturing of the LPBF samples includes higher concentrations of nickel, cobalt, molybdenum, carbon and aluminum compared to the conventional material. This suggests a higher strength and hardness due to a higher proportion of the precipitation-hardening phases Ni_3Mo and Ni_3Ti. BVAg-30 was used as a brazing filler metal with a foil thickness of 50.8 µm. The silver-based alloy contains 27% Cu and 5% Pd and has a melting range of 807–810 °C. For the samples with an increasing gap size, the foil was substituted by three wire cutoffs of diameter 800 µm of the same alloy which was placed at the larger end of the gap. In order to fix the adjusted gap, an Al_2O_3 rod of diameter one millimeter was placed after the brazing filler metal.

2.1. Experimental Design

BVAg-30 (Ag68Cu27Pd5) was used to braze nonplated as well as nickel-plated samples of any material grade combination (conventional/conventional, LPBF/conventional and LPBF/LPBF). In this regard, the nickel coating is intended to increase the joint strength due to an enhanced wetting as well as a formation of nickel-rich phases in the braze metal beside the solid solution strengthening of the silver-rich matrix. An important advantage of the chosen arc coating process for the maraging steel is given by the fact that present surface oxides will be removed, whereas nickel acts as a sealing which prevents new oxidization. In addition to the tensile strength as the decisive comparative value of the joint quality, a quasi-dynamic strength evaluation was considered taken into account that LPBF samples may contain some macroscopic imperfections which may affect the joint quality locally. Due to such defects, a reduced dynamic strength can be generally expected because of the notch effect. The strengths of the brazed samples were related to those of corresponding heat-treated solid materials. Since the microstructure of the joint will be significantly affected with the intended precipitation of nickel-rich phases in the braze metal, additional investigations of the corrosion potential were carried out.

2.2. Manufacturing of the LPBF Samples and Pretreatment of the Samples

A DMG Mori LT30 machine was used to manufacture the LPBF samples. Therefore, a laser power of 275 W and a spot size of

75 µm were set with respect to a preheat temperature of 200 °C. A strip exposure of 6 mm and a hatch distance of 115 µm were used with rotation of 67° for each layer which has a thickness of 50 µm. To prevent oxidization as far as possible, argon was used as a shielding gas (residual share of oxygen of around 0.1 vol%).

A mechanical surface grinding process was used at the joining faces for all samples which assures a sufficient evenness and a surface roughness R_z of 3.8 µm (SD 0.2). Afterward, one set of samples was nickel plated with a thickness of five micrometer in a Metaplas 20" vacuum arc evaporator by using pure nickel as a cathode (90 A, 36 V, 90 Ah). Prior to the coating, the surfaces were ion etched (100 A, −1000 V bias voltage, 3 Ah) to obtain a very high level of purity by effectively removing surface oxides and other contamination. The brazing alloy was finely ground with SiC paper immediately before brazing. All surfaces were cleaned using ethanol in an ultrasonic bath and dried by warm air.

2.3. Heat Treatment and Vacuum Brazing

The precipitation hardening heat treatment of the maraging steel was designed to be included in the brazing process cycles which were carried out in a EU80/1H 2RV vacuum furnace of IVA Schmetz GmbH as shown in **Figure 1**.

A stainless steel fixture (AISI 316L) was used to assure a concentric alignment of the cylindrical samples. The program cycle was controlled by a batch thermocouple and used a heating rate of 10 °C min^{-1} to soak the samples at 600 °C for fifteen minutes and to solution anneal as well as to braze them at 865 °C for one hour. Afterwards, the batch was cooled down to 75 °C by overpressure gas cooling with two bars of nitrogen. Subsequently, the maraging steel was precipitation hardened for three hours at 510 °C (solid samples and brazed components). Afterward, the batch was cooled to 300 °C by a controlled cool rate of 2 °C min^{-1} and then cooled again by overpressure gas cooling to room temperature.

2.4. Mechanical Testing and Microstructural Analyses

The brazed samples were machined by hard turning on a GS200MSY device (Hardinge Inc.) to tensile samples with geometry B10 × 50 according to specification DIN EN ISO 6892-1:2009-12. To turn hardened maraging steel, the application of wear-resistant coated CBN indexable inserts (VBGW 160 404) and water cooling were very helpful. The quasi-static and quasi-dynamic strength tests were carried out using a servohydraulic 250 kN pulse testing machine of type 8802MTM1021 (Instron Inc.). For tensile testing a displacement-controlled testing speed of 0.025 mm s^{-1} was used for three samples of each condition to get an average tensile strength. The half of this value was set as initial load for quasi-dynamic cycling of five samples each with a frequency of 10 MHz and an amplitude of 10 MPa. For each load level, 10^4 load cycles were performed, and then, the stress was increased by 50 MPa for the next load level until the sample failed during this increased load fatigue test.

The brazed samples were cut in the center vertically to the joint for metallographic inspection with a Mecatome T330 machine. Then one half of the brazed sample was embedded in epoxy resin, ground, and finally polished using a diamond suspension of one micrometer. Nanoindentation measurements were performed using a G200 device from Agilent Inc. on the polished cross sections by using a Berkovich tip. The mesuring field was set to ten indents wide multiplied by 25 indents for the length of the joint. An indentation depth of 0.2 µm and a space between the indents of 5 µm were chosen to achieve a maximum field resolution without affecting the subsequent indent. After the contact of the tip to the surface of the cross section was detected automatically, the load was constantly increased to the maximum indentation depth. The elastic modulus was determined from the linear top third of the unloading curve using a Poisson ratio of 0.3. The microhardness was determined similarly to the Vickers hardness test from the maximum test load and the projected area of the remaining indentation depth. The microstructural analyses were carried out using a field emission scanning electron microscope of type JSM 7001F from Jeol Inc. with an integrated EDS detector from Oxford Instruments. Prior to this, a thin layer of gold (1.5 nm) was coated on top of the cross sections with a CCU-010 sputter coater from Safematic GmbH to avoid electrical charging. For the potentiodynamic corrosion analyses, a steel wire was welded on the circumference of the remaining half of the cutted samples and insulated by a plastic hose. Then the samples were embedded in epoxy resin, ground, and polished as well as vertically placed in a solution of distilled water containing 3.0 vol% NaCl (purity 9998%). After measuring the open circuit delay for 1800 s, the samples were anodically polarized with a 600+ potentiostat of Gamry Inc. to

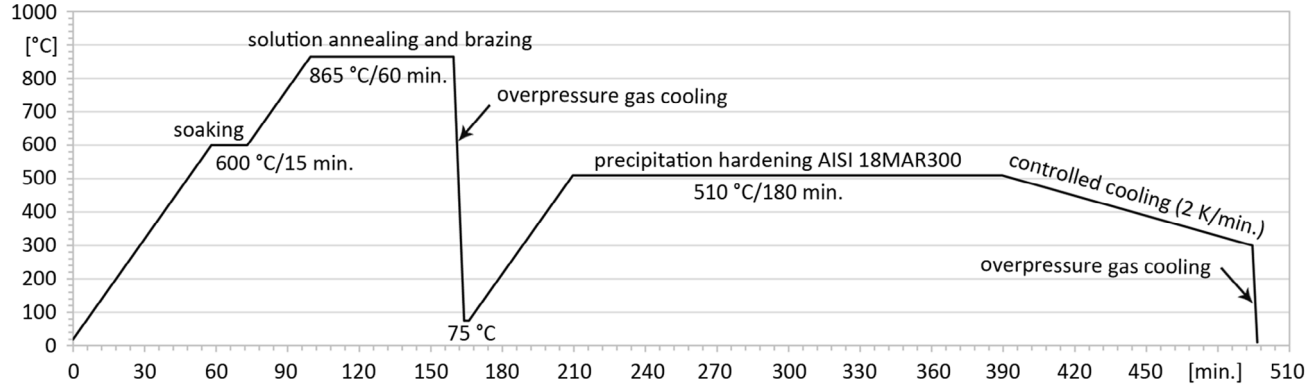

Figure 1. Schematic temperature–time–curve of the used brazing and heat-treatment process.

+0.5 V (vs ref) using a scan rate of 0.2 mV s^{-1}. An Ag/Ag-Cl electrode was used as reference and a graphite rod as counter electrode.

3. Experimental Results

3.1. Microstructure and Microhardness of the Joints

After brazing and heat treating, the nonplated samples showed a quite large bead of the braze material on one side of the circumference of the lower cylinder. This either indicates an excessive flow behavior or also a poor wetting within the brazing gap. In contrast to this, the nickel-plated samples had only a very small bead. **Figure 2** illustrates characteristic SEM images of the respective brazed joints, while the corresponding phases and their elemental composition are shown in **Table 2**.

The nonplated samples shown in the upper row had a resulting thickness of the braze metal of around 15 µm which was due to the excessive flow. Furthermore, it was clearly visible for all of these samples that severe failures of connection were present between the braze metal and the diffusion area. The main reason for this was found by means of EDS analyses which revealed that most of the palladium was consumed by the formation of the light-gray colored Cu(Pd,Ag,Fe)-solid solution phases with up to around 22 wt% Pd maximum. Because of this, the silver-rich part of the braze depletes of Pd which is again a key element for a sufficient wetting. In case of the conventional material the diffusion area was much more pronounced and showed a significantly increased liquid filler embrittlement of the base material compared to the LPBF material. In the right image, two small voids and a large interlayer defect were visible which exemplifies the size relationship of the imperfections to the joint in general.

Table 2. Elemental composition of the phases shown in Figure 1 measured by EDS (wt%).

ID	Attribution	Ti	Fe	Co	Ni	Cu	Mo	Pd	Ag
#EDS1	Cu(Pd,Ag,Fe)	0.02	4.63	0.45	1.96	61.92	0.39	22.43	8.20
#EDS2	Ag(Cu)	0.06	0.49	0.14	0.04	8.25	0.15	0.05	90.82
#EDS3	Ag(Cu,Pd)	0.39	0.32	0.06	0.78	6.64	1.52	1.01	89.28
#EDS4	DZ	0.41	48.55	8.71	34.87	0.22	4.87	2.37	–
#EDS5	NiCu(Fe,Pd,Ag)	1.10	15.66	1.43	51.67	22.86	2.11	4.11	1.06
#EDS6	FeNi-rich	0.01	43.25	5.62	38.58	6.23	4.60	1.67	0.04
#EDS7	Cu(Pd,Ag,Fe)	0.10	2.87	0.34	14.93	63.82	0.03	12.16	5.75

The joints of the nickel-plated samples shown in the lower row revealed an excellent bond at the interface which was independently of the material grade used. During brazing, the nickel coating was partially dissolved by the liquid braze and transferred into a two-banded form. Due to the high solubility within the iron-nickel system at brazing temperature, nickel diffused well into the base material and leads to an increased nickel concentration of max. 35 wt% compared to the 18 wt% of AISI 18MAR300 base material. Some of these FeNi-rich grains were dissolved and implemented in the braze metal by the effect of liquid filler metal embrittlement (dark-gray color). The two-banded phases mainly consist of NiCu(Fe,Pd,Ag) phases (mid-gray color) since this was the originally applied nickel coating. This is due to the diffusion activity and the full solubility of nickel in the copper phase of the brazing alloy. In between, the Ag(Cu,Pd) matrix of the braze metal and some Cu(Pd,Ag,Fe) phases (light-gray color) were present. For the samples using LPBF material, the two-band phases were closer to the base

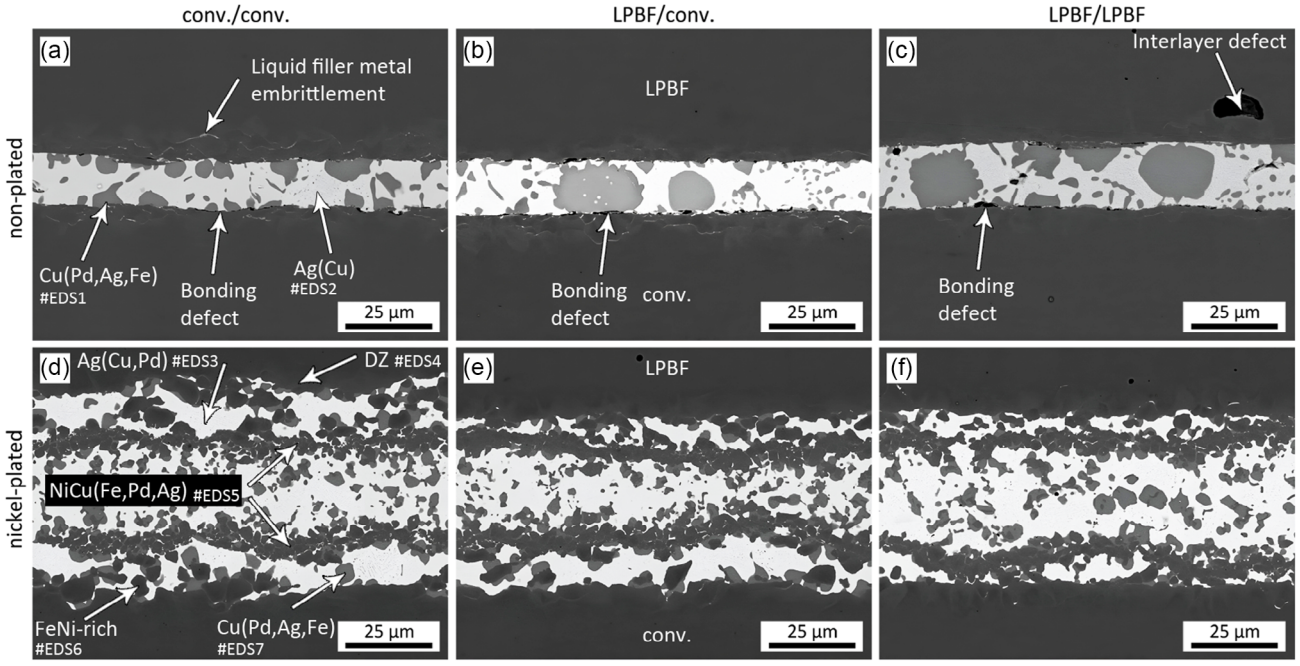

Figure 2. Characteristic SEM images in backscattered mode of the brazed joints using laser powder bed fusion processed (LPBF) and conventional (conv.) material grades: a–c) nonplated surfaces, d–f) nickel-plated surfaces.

material and not so interspersed with Ag(Cu,Pd) matrix than for the samples with a conventional material grade. However, the cross sections showed no distinct difference for the diffusion area in dependence of the material grade used, nor any influence of imperfections of LPBF material on the local joint quality.

Due to the limited wetting capability the samples with an increasing gap size and the nonplated surface showed melting but just a very small flow behavior in the gap so that these results were not investigated further. In contrast, the nickel-plated samples with an increasing gap size showed an excellent flow behavior into the small gap opposite to the applied brazing filler metal. **Figure 3** illustrates the main results of these investigations.

Only above a gap size of around 115 µm, there was additionally the eutectic phase present in the center of the joint (Figure 3a) which was surrounded by Ag(Cu)-solid solution matrix (white color) and Cu(Pd,Ag,Fe)-phases (light-gray color). At large gap sizes, there was a full eutectic microstructure in the center of the joint. The two-band phases were always present in the vicinity of the diffusion area regardless of the gap width. The dissolution mechanism of the nickel coating was observed at the rim of the flow area (Figure 3b). It was found that the coating was dissolved in the base material as well as transferred to the copper-rich phases of the braze metal. This is due to the high solubility of nickel in iron and copper at the maximum process temperature. Additionally, it was the Ag(Cu,Pd) phase to be responsible for the liquid filler metal embrittlement of the base material grains and the coating as well. However, near the zero gap, the two-band phases were very close together with a minimum of Ag(Cu,Pd) matrix in between. **Figure 4** illustrates the characteristic results of the nanoindentation measurements for a LPBF/conv. joint.

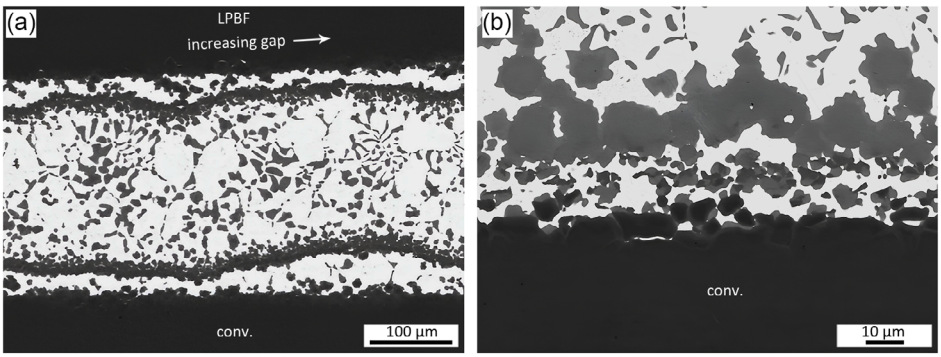

Figure 3. Characteristic SEM images in backscattered electron mode of brazed samples with an increased gap size a) two-banded microstructure with eutectic phases in the joint center for large gap sizes; b) dissolution of the nickel coating and the base material grains.

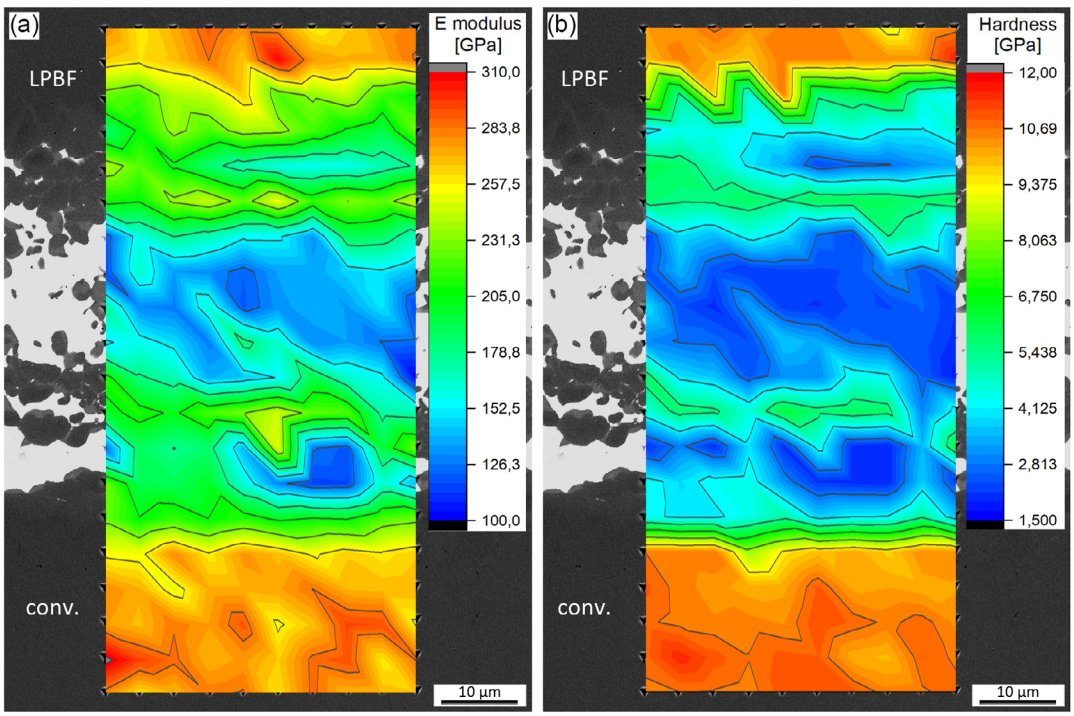

Figure 4. a) Elastic modulus and b) microhardness of a hybrid joint using laser powder fusion processed (LPBF) and conventional (conv.) material grades as well as nickel-plated surfaces.

Based on the elastic and plastic deformation during nanoindentation, an attempt was made to draw conclusions about the strength behavior of the joint. In general, the elastic modulus increases with the resistance that a material offers to its elastic deformation. As it can be seen in the left image, the precipitation hardened maraging steel has a high elastic modulus of 265 GPa in average, while the Ag(Cu,Pd) matrix of the braze metal was just 140 GPa in average. It was found that the elastic modulus was significantly decreased to in average 215 GPa for the diffusion area of the steel, which was mainly enriched with nickel due to the coating and to in average 195 GPa for the two-banded NiCu(Fe,Pd,Ag) phases. The Cu(Pd,Ag,Fe) phases had an average value of 170 GPa. Although the microhardness only allows limited conclusions regarding strength, it tends to describe the resistance to plastic deformation of a local phase quite well for brazed joints. Generally, the hardness distribution showed a similar behavior as the elastic modulus. The Ag(Cu,Pd) matrix was by far the softest phase of the joint and thus, it can be stated in a total view that as the joint is loaded axially, the elastic as well as the plastic deformation will start at the matrix. However, it can be also seen that the two-banded phases should increase the joint strength significantly. As the microstructures were very similar, there was no significant dependence on material grade used on the elastic modulus and the microhardness.

3.2. Quasi-Static and Quasi-Dynamic Strength Behavior

The results obtained by the quasi-static and the quasi-dynamic strength testing are illustrated in **Figure 5**.

The nonplated conv./conv. samples showed an average tensile strength of 655 MPa (SD: 60) with the quasi-dynamic strength being significantly lower and with a very high standard deviation (455 MPa, SD: 117). As one can see, the results of the nonplated samples using LPBF as material grade were proved to be unsuitable since the quasi-static strength was very poor and most of the samples for the cycle test broke apart during turning of the tensile test geometry (LPBF/conv. all samples, LPBF/LPBF two samples). In contrast to this, the results of the nickel-plated samples revealed a clear dependence of the material used on the strength behavior. In detail, the tensile strength was significantly increased with the utilization of LPBF material (conv./conv. 627 MPa SD: 41, LPBF/conv. 764 MPa SD: 89, LPBF/LPBF 825 MPa SD: 15). The quasi-dynamic strength of the nickel-plated samples corresponded in principle to the respective tensile strength. In case of the LPBF/LPBF samples, the average quasi-dynamic strength was lowered by two samples with a quite low strength leading to the high standard deviation. The average tensile strength of the conventional solid maraging steel in the precipitation hardened condition was R_m 2086 MPa (SD: 1) whereby the quasi-dynamic strength was comparable (2096 MPa SD: 21). In contrast, the average tensile strength (1905 MPa SD: 85) and the average quasi-dynamic strength (R_{ILF} 1845 MPa SD: 161) of the LPBF solid material were significantly lower. In relation to this, the tensile strength of the brazed samples with nickel coating was around 30% (conv./conv.), 40% (LPBF/conv.) and 43% (LPBF/LPBF).

The fracture behavior was evaluated on the surface as well as on cross sections of the brazed tensile samples. All samples with a nonplated surface fractured at the interface of the braze metal and the diffusion area. In contrast, all nickel-plated samples fractured in the center of the joint within the Ag(Cu,Pd) matrix as predicted by the nanoindentation results. **Figure 6** illustrates this characteristic fracture behavior for a hybrid LPBF/conv. joint with nickel-plated surfaces.

It the left images, it can bee seen that the fracture occurred either just above the two-banded phases or exactly in the center of the joint. However, the Ag(Cu,Pd) matrix in between the phase band and the diffusion area was not damaged in general. In detail, there were some defects visible in the joint in the vicinity of the LPBF part (black color) which could have been significantly stretched by the mechanical loading during tensile testing. However, such defects were not visible for the unloaded samples. In the right image, the effect of an interlayer defect at the joint face was present which was quite rare in the cross sections. It was found that an unmolten powder particle of the LPBF process was coated with nickel and wetted by the braze within this large interlayer defect. Analyses of the fractured surfaces of the brazed LPBF parts in the topview revealed that several of such defects were present. As a result, a direct relationship of the base material imperfections to the joint quality could be demonstrated which was

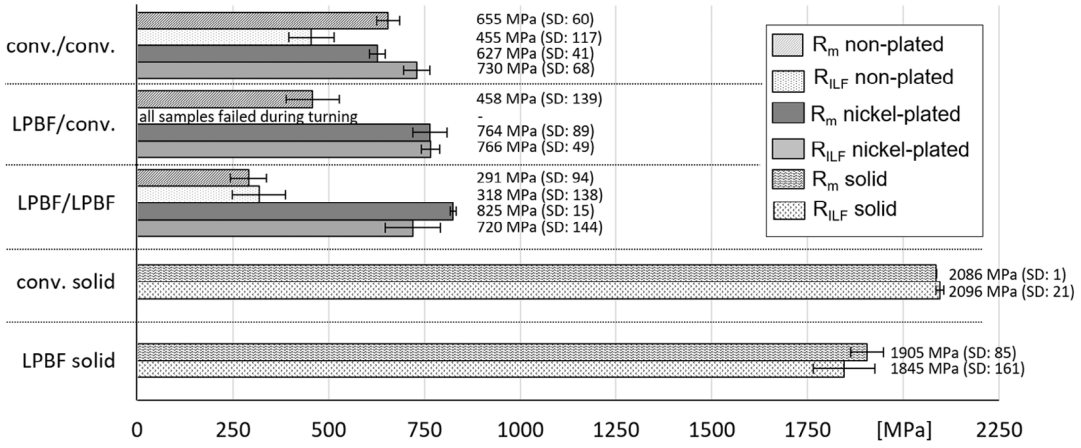

Figure 5. Quasi-static (R_m) and quasi-dynamic strength (R_{ILF}) results of brazed joints and heat-treated solid with respect to the material grade used.

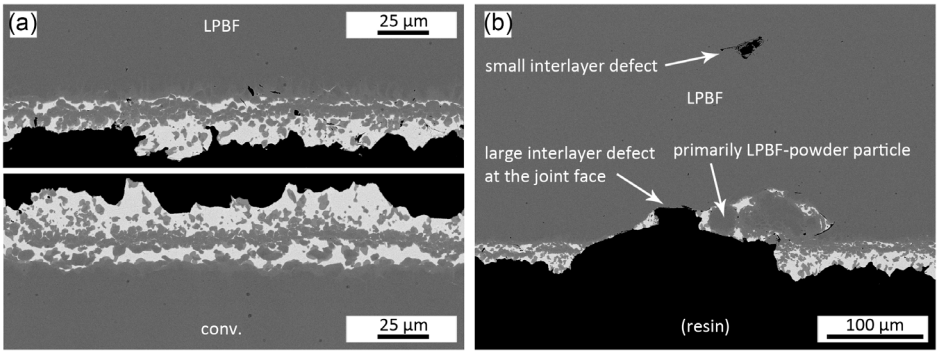

Figure 6. SEM images in backscattered electron mode of the characteristic fracture behavior: a) nickel-plated samples, b) effect of imperfections in the laser powder fusion prcessed component (LPBF) on the fracture behavior.

found to be the main reason for the low quasi-dynamic strength of the two LPBF/LPBF samples mentioned earlier.

3.3. Corrosion Behavior

The metallurgical effect of the potentiodynamic corrosion measurements is shown in **Figure 7**.

The open-circuit delay was in average −0.318 V (SD: 22.4), whereby no significant difference was found depending on the material grade used or the surface condition (nonplated, nickel plated). After polarization, the steel surfaces of the cross sections appeared black. In detail, the corrosion damage for the conventional material grade was observed in particular at the prior austenite grain boundaries (visible as cracks), which was superimposed by a planar attack of the grain. Except of a coarser and more elongated morphology of the areas between the cracks, the corrosion behavior of the LPBF part was similar. In detail, there was an enrichment of nickel visible at the interface of the joint with nickel plating which is due to to a higher diffusion activity at the prior austenite grain boundary. The diffusion zone at the LPBF part showed a much smaller morphology of these nickel enrichements which is due to the finer microstructure of LPBF material. Therefore, it was not possible to analyze whether the diffusion zone was attacked, but it is more likely that the steel between the enrichments of nickel was corroded. In summary, the results prove that the nickel platings does not reduce the corrosion resistance of the brazed joints while the maraging steel was corroded severely and largely independent of the material grade used.

4. Conclusion

The following is a summary of the key findings. It could be proven that vacuum brazing of LPBF processed components was excellent controllable if the joint surfaces were coated by arc-PVD with nickel. In this process, the oxide layer of the maraging steel, which is very difficult to wet, was removed by ion etching and sealed against reoxidation with nickel that is easy to wet. Furthermore, it was demonstrated that the nickel coating was very beneficial to enhance the joint strength which was due to a formation of two-banded phases in the microstructure of the brazed joint. Thus, the fracture mirror shifted from the interface for the nonplated samples to the center of the joint within the Ag(Cu,Pd) matrix for the nickel-plated ones. Additionally, it was shown that the fracture behavior is predictable by nanoindentation in general. It was demonstrated that the material grade used for brazing (LPBF, conventional) affects the quality of the brazed joint since major imperfections of the LPBF material at the joint face were not closed by the arc-PVD coating. As a consequence, the braze metal was not able to fill-up the volume of the imperfections. In contrast to these local events, the microstructure of the joint was largely independent of the material grade used for the nickel-plated samples. However, it was shown that the joint strength increased significantly with the utilization of LPBF

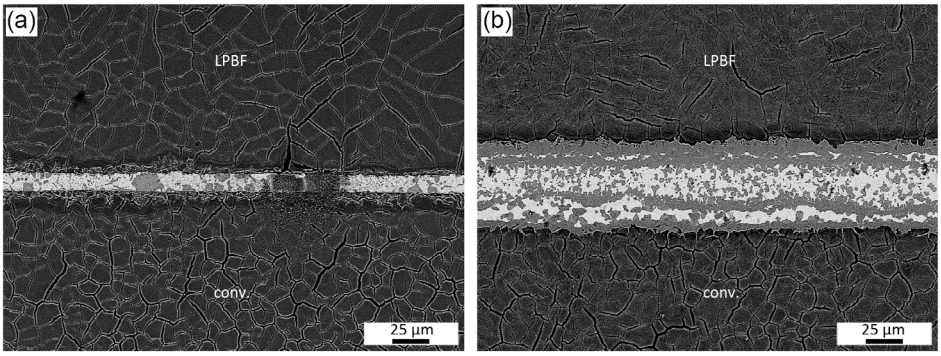

Figure 7. Characteristic SEM image in backscattered electron mode of anodically polarized joints in 3.0 vol% NaCl solution for brazed hybrid samples of laser powder fusion processed (LPBF) and conventional (conv.) material grades: a) nonplated surfaces, b) nickel-plated surfaces.

material (conv./conv. 627 MPa SD: 41, LPBF/conv. 764 MPa SD: 89, LPBF/LPBF 825 MPa SD: 15). The reason for this is seen in the fact that the two-banded phases were not so interdispersed with Ag(Cu,Pd) matrix than for joints using a conventional material grade. Furthermore, the strength of the nickel-plated joints was not reduced by quasi-dynamic loading. It was observed that the quasi-dynamic strength was in particular significantly reduced by a higher number of imperfections in the LPBF material. Anyway, the results obtained using BVAg-30 prove that the joint strength is mainly limited by the amount of the Ag(Cu,Pd) matrix. Thus, it will be a promising approach to investigate the effect of a thinner brazing foil (e.g., 25 μm) in future so that the two-banded phases were closer to each other. Furthermore, the effect of the coating thickness and the dwell time on the formation and distribution of the two-banded phases within the Ag(Cu,Pd) matrix is of interest, which may affect the strength of the joint significantly. If a considerably higher joint strength is required for the technical field of application of the ultrahigh strength maraging steel hybrids (LPBF/conv.), our previous studies recommend the utilization of AuNi18 brazing alloy (904 MPa, SD: 38), which does not require a nickel coating or to manufacture the hybrid directly by the LPBF process on top of a conventional material without brazing (1998 MPa, SD:62). Finally, it was demonstrated that the microstructure of the brazed joints using BVAg-30 was not affected by a 3.0 vol% NaCl solution during potentiodynamic testing. In contrast, AISI 18MAR300 was severely corroded, which was largely independent on the material type used.

Acknowledgements

The contents presented were conducted within project TI 343-162-1 "Brazeability of similar hybrid joint compounds consisting of additively manufactured and conventional material grades", which is founded by the German Research Foundation (DFG). The sponsorship and support are gratefully acknowledged. Many thanks to Maxwell Hein and Kay-Peter Hoyer of the Institute of Materials Science from University Paderborn for the manufacturing of the LPBF material.

Open Access funding enabled and organized by Projekt DEAL.

Conflict of Interest

The authors declare no conflict of interest.

Data Availability Statement

The data that support the findings of this study are available from the corresponding author upon reasonable request.

Keywords

corrosion behavior, joint strength, LPBF, maraging steels, microstructures, vacuum brazing

Received: February 22, 2023
Revised: June 19, 2023
Published online: August 13, 2023

[1] I. E. Klein, A. E. Yaniv, J. Sharon, *Appl. Surf. Sci.* **1982**, *14*, 351.
[2] L. Zhu, A. Al-Sakeeri, F. Lenrick, O. D. Berg, P. Sjödin, A. A. Zakharov, A. Knutsson, A. Mikkelsen, *Surf. Interface Anal.* **2022**, *54*, 99.
[3] C. Strauß, L. Wegewitz, S. Schöler, U. Holländer, K. Möhwald, W. Maus-Friedrichs, *Steel Res. Int.* **2020**, *91*, 1900568.
[4] V. X. L. Filho, I. F. Barros, H. F. G. de Abreau, *Mater. Res.* **2017**, *20* 10.
[5] H. F. Rush, *NASA Technical Memorandum 85816*, NASA (National Aeronautics and Space Administration), Hampton, VA **1984**.
[6] G. Saul, J. A. Roberson, A. M. Adair, *Metall. Trans.* **1970**, *1*, 383.
[7] H. Hou, L. Qi, Y. H. Zhao, *Mater. Sci., Eng. A* **2013**, *587*, 209.
[8] J. F. Bradshaw, P. G. Sandefur, C. P. Young Jr., *NASA Technical Memorandum 104075*, NASA (National Aeronautics and Space Administration), Hampton, VA **1991**.
[9] J. R. Davis, *Heat Treating*, Vol. *4*, ASM International, Novelty, OH **2007**.
[10] C. R. Shamanta, R. Narayanan, K. J. L. Iyer, V. M. Radhakrishnan, S. K. Seshardi, S. Sundararajan, S. Sundaresan, *Mater. Sci. Eng., A* **2007**, *287*, 43.
[11] R. Casati, J. N. Lemke, A. Tussi, M. Vedani, *Metals* **2016**, *6*, 218.
[12] A. M. Hall, C. J. Slunder, *The Metallurgy, Behavior, and Application of the 18-percent Nickel Maraging Steels—A Survey*, NASA (National Aeronautics and Space Administration), Washington, DC **1968**.
[13] S. Afkhami, M. Dabiri, S. Habib Alavi, T. Björk, A. Salminen, *Int. J. Fatigue* **2019**, *122*, 72.
[14] L. Thijs, J. Van Humbeeck, K. Kempen, E. Yasa, J. P. Kruth, M. Rombouts, *Virtual Phys. Prototyping* **2012**, 297.
[15] K. Kempen, E. Yasa, L. Thijs, J. P. Kruth, J. Van Humbeeck, *Phys. Procedia* **2011**, *12*, 255.
[16] R. Hoelker, A. E. Tekkaya, *J. Adv. Manuf. Technol.* **2016**, *83*, 1209.
[17] W. Tillmann, L. Wojarski, T. Henning, *Weld. World* **2021**, *65*, 1323.
[18] M. Schröder, B. Falk, R. Schmitt, *Procedia CIRP* **2015**, *30*, 311.
[19] M. Oyesola, K. Mpofu, N. Mathe, *Procedia Manuf.* **2019**, *35*, 155.
[20] A. Ascari, A. Fortunato, E. Liverani, A. Gamberoni, L. Tomesani, *Phys. Procedia* **2016**, *83*, 839.
[21] L. Kučerová, I. Zetková, Š. Jeníček, K. Burdová, *Addit. Manuf.* **2020**, *32*, 101108.
[22] H. Azizi, R. Ghiaasiaan, R. Prager, M. H. Ghoncheh, K. A. Samk, A. Lausic, W. Byleveld, A. B. Phillion, *Addit. Manuf.* **2019**, *27*, 389.
[23] I. Reinkensmeyer, R. Blank, O. Herrmann, *Schweißen Schneiden* **2019**, *71*, 214.
[24] W. Tillmann, L. Wojarski, T. Henning, M. Möbus, in *Proc. 12th Inter. Conf. on Brazing, High Temperature Brazing and Diffusion Bonding LÖT 2019*, Vol. *353*, DVS Media GmbH, Düsseldorf, Germany **2019**, pp. 18–25.
[25] D. Feil, F. Wetzl, A. Fix, T. Herberholz, G. Michael, G. Schmitz, *DVS-Reports, 325, Brazing, High Temperature Brazing and Diffusion Bonding*, DVS Media GmbH, Düsseldorf, Germany **2016**, pp. 139–143.
[26] R. D. Berry, *Weld. Met. Fabr.*, *3*, 93, **1965**.
[27] L. Kučerová, I. Zetková, A. Jandová, M. Bystrianský, *Mater. Sci. Eng., A* **2019**, *750*, 70.
[28] S. Giganto, P. Zapico, M. Á. Castro-Sastre, S. Martínez-Pellitero, P. Leo, P. Perulli, *Procedia Manuf.* **2019**, *41*, 698.
[29] J. A. M. Ferreira, L. M. S. Santos, J. da Silva, J. M. Costa, C. Capela, *Procedia Struct. Integrity* **2016**, *1*, 126.
[30] Y. Huang, T. G. Fleming, S. J. Clark, S. Marussi, K. Fezzaa, J. Thiyagalingam, C. L. A. Leung, P. D. Lee, *Nat. Commun.* **2022**, *13*, 1170.
[31] W. Tillmann, T. Henning, L. Wojarski, *IOP Conf. Ser.: Mater. Sci. Eng.* **2018**, *373*, 012023.
[32] E. Bouzakis, A. Arvanitidis, F. Kezelis, G. Maliaris, N. Michailidis, *Procedia CIRP* **2020**, *87*, 469.